

# Entanglement topography of large-scale quantum networks

Md Sohel Mondal and Siddhartha Santra\*

Department of Physics and CoE-QUICST, Indian Institute of Technology Bombay, Mumbai, Maharashtra 400076, India

Dov Fields and Vladimir S. Malinovsky  
US Army Research Laboratory, Adelphi, Maryland 20783, USA

Large-scale quantum networks, necessary for distributed quantum information processing, are posited to have quantum entangled systems between distant network nodes. The extent and quality of distributed entanglement in a quantum network, that is its functionality, depends on its topology, edge-parameter distributions and the distribution protocol. We uncover the parametric entanglement topography and introduce the notion of typical and maximal viable regions for entanglement-enabled tasks in a general model of large-scale quantum networks. We show that such a topographical analysis, in terms of viability regions, reveals important functional information about quantum networks, provides experimental targets for the edge parameters and can guide efficient quantum network design. Applied to a photonic quantum network, such a topographical analysis shows that in a network with radius  $10^3$  kms and 1500 nodes, arbitrary pairs of nodes can establish quantum secure keys at a rate of  $R_{sec} = 1$  kHz using 1 MHz entanglement generation sources on the edges and only entanglement swapping at the nodes.

A quantum network (QN) [1–3] is a paradigm-changing type of communication network in which long-range entanglement is the essential resource for a range of classically impossible tasks ranging from unconditionally secure communications to distributed quantum computation [2, 4, 5]. The design of these networks in terms of size, topology and functionality is rapidly maturing along with the development of quantum hardware [3]. Recent works have, nevertheless, shed light on some of their expected network and information-theoretic properties such as deviation from the small-world property [6], capacity phase transitions [7], noise-robustness [8] and percolation thresholds [9].

Here, we address an important practical question pertaining to the structure of a QN: what is the statistically viable region for a quantum information processing (QIP) task, such as (but not limited to) quantum key distribution (QKD), in a QN within which the entanglement connection between any pair of source-destination ( $S$ - $D$ ) nodes satisfies the parameter thresholds required for the task. As estimate of this size can serve as a network characteristic useful for assessing functionality and designing an efficient network before it is simulated and constructed [10–12]. To the best of our knowledge, however, such a metric has previously not been obtained.

Large-scale QNs have a web-like structure with multiple possible paths between any pair of  $S$ - $D$  nodes [13]. Associated with each path is a set of parameters (obtained by appropriate fusion of edge parameters) that captures the various physical attributes of the entanglement distribution scheme such as the concurrence of the distributed state, the probability of success, the time required etc. In this multi-parameter scenario, in general, no single path optimizes all the elements of the parameter set simultaneously [14, 15]. Rather, a set of distinguished Pareto-optimal paths exists such that moving from one to the other some parameters improve while others degrade. Moreover, the parameters obtained along multiple alternate paths between the same pair of  $S$ - $D$  nodes may also be combined using entanglement purification - potentially improving the

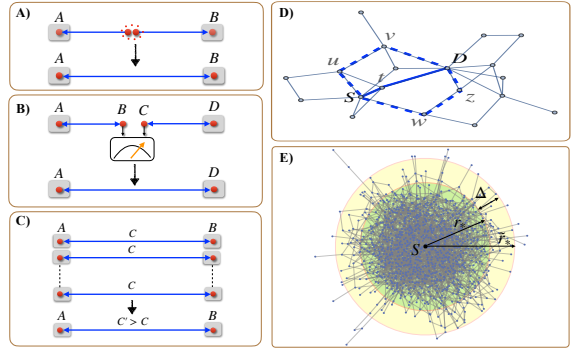


FIG. 1. (A-D) Quantum network operations and (E) entanglement topography of the network. (A) Entanglement generation between adjacent nodes  $A, B$  (B) Entanglement swapping to transform network edge-entanglement to path-entanglement (C) Entanglement purification to increase network-edge concurrence (D) Multi-path entanglement purification over distinct paths between the same  $S$ - $D$  node pair with the solid Blue line showing the shortest graph path and dashed Blue lines showing alternate graph paths.

entanglement connection between  $S$ - $D$  via multi-path entanglement routing and purification [9, 16, 17]. To obtain the viability region in a QN, the challenge, therefore, is to appropriately characterise the entanglement connection between any  $S$ - $D$  node pair given the allowed network operations.

Here, we introduce the notion of typical and maximal viable region (TVR and MVR) for a QIP task in a general model of a large-scale QN. These regions naturally emerge via an exploration of a network's bipartite-entanglement topography (spatial distribution) about a random network node,  $S$  based on local operations and classical communication (LOCC) between the network nodes. Intuitively, for any destination node within a source node's TVR the upper bound on the probabil-

ity of their entanglement connection to satisfy the parameter thresholds for a specific QIP task is equal to one. Outside of this region, in the MVR, the probability of satisfying the thresholds is upper bounded strictly away from unity. The size of the TVR or MVR is a characteristic of the network relative to a specific QIP task and is determined by the statistical distribution of the network-edge parameters. However, it can be significantly enhanced by allowing more complex network operations for suitable network edge-parameter ranges. We elucidate these ideas in the following starting, first, from a description of the model for a large-scale QN.

*Quantum network model:* We consider a QN defined on an underlying graph  $G(V, E)$  where  $V$  is the set of network nodes and the edges  $e \in E$  represent entangled links in terms of two-qubit states  $\rho_e$  given by,

$$\rho(q_e) = (1 - q_e)|\phi^+\rangle\langle\phi^+| + q_e \frac{\mathbf{1}_4}{4}, \quad (1)$$

with  $|\phi^+\rangle = (|00\rangle + |11\rangle)/\sqrt{2}$ , which are a one-parameter family of mixed states with  $0 \leq q_e \leq 1$ , widely considered in several recent QN models [7, 18–20]. The concurrence, a bipartite-entanglement measure, of states in Eq. (1) is linearly related to the parameter,  $q_e$ , via  $c(\rho_e) = \text{Max}(0, 1 - 3/2q_e)$ , therefore, such states are quantum entangled whenever,  $q_e < 2/3$ , equivalently,  $\langle\phi^+|\rho_e|\phi^+\rangle > 1/2$ .

The physical attributes of the network edges are described by a set of random-valued, positive semi-definite, edge-parameters,  $\{\mu_i\}_{i=1}^n$ , with  $n$ -the number of parameters that specify the network, such as the concurrence, probability of edge-entanglement, link latency etc. with their own independent distributions,  $\text{Dist}(\mu_i)$ . A family of QNs,  $\tilde{Q}$ , is then fully specified given the tuple,

$$\tilde{Q} := \{G(V, E), \text{Dist}(\mu_1), \text{Dist}(\mu_2), \dots, \text{Dist}(\mu_n)\}, \quad (2)$$

along with an entanglement distribution scheme such as the one we now describe.

The entanglement distribution scheme here proceeds via a sequence of three probabilistic LOCC network operations: entanglement generation (EG), entanglement swapping (ES) and entanglement purification (EP) all of which follow a geometric distribution in the number of trials before succeeding. While EG establishes short-range entangled states over the network edges [21], ES increases the range of entangled states by entangling even those nodes that have never directly interacted [22]. The quality of distributed entanglement can be further enhanced by a final entanglement purification (EP) step [23, 24] which purifies the two-qubit entangled states distributed along distinct alternate paths between a pair of  $S$ - $D$  nodes, see Fig. (1). Importantly, all network operations preserve the form Eq. (1) upto local unitary transformations.

*Characterizing entanglement connections in the network:* The entanglement connection between a pair of  $S$ - $D$  nodes over an entanglement distribution path,  $\mathcal{P}$ , in such a QN is fully described via a  $n$ -tuple,  $(\mu_{1,\mathcal{P}}, \mu_{2,\mathcal{P}}, \dots, \mu_{n,\mathcal{P}})$ , of random valued path-parameters,  $\mu_{i,\mathcal{P}}$ , that are functions of the

edge-parameters along the path. Here, we simplify the discussion by characterising every path via a 2-tuple,  $(C_{\mathcal{P}}, P_{\mathcal{P}})$ , respectively of the concurrence and probability for a path of arbitrary length,  $l$ . We use the path label,  $\mathcal{P}$ , and its length,  $l$ , interchangeably since the statistical properties of path-parameters depends only on its length in addition to the statistical properties of the edge-parameter distributions. We formulate the latter in terms of their maximum, mean and minimum as,  $\text{Max}(\mu_i) = (1 - a_i\delta_i)$ ,  $0 \leq a_i < 1$ ,  $\overline{\mu_i} = (1 - \delta_i)$ ,  $0 \leq \delta_i \leq 1$ ,  $\text{Min}(\mu_i) = (1 - b_i\delta_i)$ ,  $1 \leq b_i \leq 1/\delta_i$  where  $\mu_i$  is the random variable denoting the edge-concurrence (probability) for  $i = 1(2)$ . The quantity,  $\delta_i$  is a measure of the closeness of the mean to the maximum (1 in case of concurrence and probability) of the random valued edge parameters. The quantity,  $(b_i - a_i) \geq 0$ , then is a measure of the homogeneity of the distribution becoming zero for a homogenous parameter distribution - where all edges have identical parameters; while larger values indicate increasing inhomogeneity in the distribution of the parameter values over the network edges.

In such a QN, the average path parameters of the entanglement connection achieved by ES at all intermediate nodes along a path of length  $l$  is given by,

$$\overline{C}_l = \text{Max}\left[0, \frac{3}{2}(1 - (2/3)\delta_1)^l - \frac{1}{2}\right], \overline{P}_l = (1 - \delta_2)^l, \quad (3)$$

which only depend on the mean values of the edge-parameters via  $\delta_{1,2}$  and decrease monotonically with path length,  $l$ . For large-scale networks the edge parameters must approach their maximum allowed values as,  $\delta_{1,2} \sim 1/\text{Poly}(N)$ , for graph size  $|V| = N$ . In this case, for short paths,  $l \ll \min(1/\delta_1, 1/\delta_2)$ , we find that,  $\overline{C}_l \simeq (1 - l\delta_1)$  and  $\overline{P}_l \simeq (1 - l\delta_2)$  implying that the path-parameters decrease linearly with  $l$ . Whereas for long paths,  $l \gtrsim \min(1/\delta_1, 1/\delta_2)$ , they are exponentially suppressed,  $\overline{C}_l \sim (3/2)e^{-(2/3)\delta_1 l} - (1/2)$ ,  $\overline{P}_l \sim e^{-\delta_2 l}$  (see Fig. 2 in Supp. mat.).

*Topographic length-scales in the network:* The scaling of the entanglement connection length, from Eq. (3), suggests that subgraphs of the network can be topographically classified into distinct regions based on high- or low- values of the path parameters in correlation with the graph distance relative to an arbitrary network node. Thus, we can define,  $G_S \subseteq G$ , as the largest subgraph centered at a random node,  $S \in V$ , such that  $S$ - $D$  pairs with  $D \in G_S$  have an entanglement connection with on-average non-zero value of the concurrence and path probability above an experimentally significant cutoff probability  $0 \leq \xi \leq 1$ . The size of  $G_S$  in terms of its radius about the central node  $S$  yields two length-scales,

$$r^C = (3/2)\ln 3/\delta_1, \quad r^P = \ln(1/\xi)/\delta_2, \quad (4)$$

which determine the maximum radius of the entanglement connection that may be established in the network. The entanglement radius,  $r^C$  and the connection radius,  $r^P$ , are the average maximum distances between two network nodes that can have non-zero bipartite entanglement and experimentally significant probabilities respectively.

The topographic length scales, Eq. (4), readily yield the scaling of the edge-parameter means with graph size for arbitrary network topologies. Requiring, the radius of a network graph,  $r$ , to equal the entanglement and connection radius, that is  $r = r^C = r^P$ , we get,  $\overline{\mu_1} \sim 1 - (3/2) \ln 3/r$  and  $\overline{\mu_2} \sim \xi^{1/r}$  with  $r = r_{ER}, r_{SF}$ , where for Erdos-Renyi networks,  $r_{RN} \sim \ln N$ , and for scale-free networks,  $r_{SF} \sim \ln \ln N$  [25]. From the implementation point of view this implies that for a large-scale QN with  $N = 10^6$  nodes the demand on the mean edge-parameters are  $(\overline{\mu_1}, \overline{\mu_2})_{ER} = (0.88, 0.72)$  and  $(\overline{\mu_1}, \overline{\mu_2})_{SF} = (0.37, 0.17)$ , giving experimental target values in the two topologies.

*Thresholds for QIP tasks:* QIP tasks require the path-parameters in the multiparametrized entanglement connection to be above certain thresholds. For example, for QKD a concurrence of,  $C_{S-D} \geq 0.78$ , between a  $S$ - $D$  pair is needed to obtain a non-zero finite secure key rate [19]. Assuming that the entangled photon sources in the network operate at a rate of,  $R_{eps} = 1\text{MHz}$ , the edge states are isotropic with concurrence,  $C = 0.80$ , and the desired rate of secure key generation is,  $R_{sec} = 1\text{kHz}$ , then the probability of the entanglement connection needs to be at least,  $P \geq R_{sec}/\{R_{eps} * (1 - 2h[(1 - C)/2])\} \approx 1.6\%$ , where  $h[x]$  is the binary entropy function. Thus, for QKD entanglement connections with,  $(C_l, P_l) \geq (c_*, p_*) = (0.8, 1.6\%)$ , between any  $S$ - $D$  pair will be necessary and such  $D$ -nodes which satisfy the desired thresholds are part of the viable region for QKD relative to a given  $S$ .

*Typical viable region:* We define the TVR,  $V_S$ , as the connected subgraph,  $G_S$ , centered at a random graph node,  $S$ , such that on-average the entanglement connection between,  $S$  and any other node  $D \in G_S$ , along the shortest graph path (SGP) meets the multiparameter thresholds for the given QIP task. That is,

$$V_S := \{G_S \subseteq G \mid \mathcal{D}(S, D) \leq r_* \forall D \in G_S\}, \\ r_* : \text{largest } l \text{ s.t. } (\overline{C}_l, \overline{P}_l) \geq (c_*, p_*), \quad (5)$$

where  $\mathcal{D}(S, D)$  is the graph distance between  $S, D$ . Note that within  $V_S$ , Markov's inequality applied to the random variable,  $X_{S-D}$  for  $X = C, P$ , which is the path parameter between any,  $D \in V_S$ , and the central node,  $S$ , implies that,  $\Pr(X_{S-D} \geq x_*) \leq \text{Min}[1, \overline{X}_{S-D}/x_*] = 1$  for  $x_* = c_*, p_*$ .

The TVR,  $V_S$ , may be visualised as the intersection of the analogously defined independent TVRs,  $V_S^C$  and  $V_S^P$ , for the path concurrence and probability with respective radii,  $r_*^C$  and  $r_*^P$  - the radius of,  $V_S$ , being the smaller of the two. Thus,  $r_* = \text{Min}\{r_*^C, r_*^P\}$  can be expressed as,

$$r_* = \text{Min}\{r^C(1 - \frac{\ln(1 + 2c_*)}{\ln 3}), r^P \frac{\ln p_*}{\ln \xi}\} \quad (6)$$

for a task with a given set of thresholds  $(c_*, p_*)$  with  $0 \leq c_* \leq 1, \xi \leq p_* \leq 1$ . For  $(c_* \rightarrow 1, p_* \rightarrow 1)$  both  $r_*^C, r_*^P \rightarrow 0$ , whereas, when  $(c_* \rightarrow 0, p_* \rightarrow \xi)$  the radii  $r_*^C \rightarrow r^C, r_*^P \rightarrow r^P$  for all  $\delta_{1,2} > 0$ . Thus, the radius of the TVR can be as large as the smaller of the entanglement radius,  $r^C$ , or connection

radius,  $r^P$ , for small values of the thresholds whereas for high thresholds the TVR can be very small.

Importantly, the size of the TVR given by,  $r_*$ , is translationally invariant over the network nodes and is a characteristic of the *entire* network. However, the utility of a specific node in a network of given topology as the source,  $S$ , for a QIP task is determined by the degree of that node. For example, the TVR around a 'hub' in a scale-free network is more useful as a  $S$ -node because its high degree allows more nodes to populate its TVR compared to an 'end'-node in the same network though both have the same radius  $r_*$  for their TVRs.

*Maximal viable region:* The MVR,  $\tilde{V}_S$ , is an extension of the TVR for a given task such that for any node,  $D \in \tilde{V}_S$ , the maximum probability of meeting the entanglement connection threshold between  $S$ - $D$  is lower bounded away from zero - even though on-average the thresholds are not met. The MVR is obtained by relaxing the typical viability condition in Eq. (5). Mathematically, the MVR,  $\tilde{V}_S$ , for a task is the largest subgraph,  $\tilde{G}_S$ , where the parameters of the entanglement connection along the SGP between any  $D \in \tilde{G}_S$ , and, the centre,  $S$ , have a probability of satisfying the parameter thresholds with an upper bound of at least  $\epsilon^X$  where  $1 \geq \epsilon^X \geq 0$  and  $X = C, P$ . That is,

$$\tilde{V}_S := \{\tilde{G}_S \subseteq G \mid \mathcal{D}(S, D) \leq \tilde{r}_* \forall D \in \tilde{G}_S\} \\ \tilde{r}_* : \text{largest } l \text{ s.t. } \text{Max}(\Pr(X_l \geq x_*)) \geq \epsilon^X. \quad (7)$$

The MVR,  $\tilde{V}_S$ , is the intersection of the analogously defined independent MVRs,  $\tilde{V}_S^C$  and  $\tilde{V}_S^P$ , for the two path parameters with radii,  $\tilde{r}_*^C$  and  $\tilde{r}_*^P$ . The radius,  $\tilde{r}_* = \text{Min}\{\tilde{r}_*^C, \tilde{r}_*^P\}$ , of  $\tilde{V}_S$  being the smaller of the two,

$$\tilde{r}_* = \text{Min}\{r^C(1 - \frac{\ln(1 + 2c_*\epsilon^C)}{\ln 3}), r^P \frac{\ln p_*\epsilon^P}{\ln \xi}\}, \quad (8)$$

for a task with thresholds  $(c_*, p_*)$  and given  $\epsilon^C, \epsilon^P$ . Assuming,  $\epsilon^C = \epsilon^P = \epsilon$ , for simplicity, when  $(c_* \rightarrow 1, p_* \rightarrow 1)$  both  $r_*^C, r_*^P \rightarrow 0$  for  $\epsilon \rightarrow 1$  whereas,  $r_*^C \rightarrow r^C, r_*^P \rightarrow r^P$ , for  $\epsilon \rightarrow 0$ . On the other hand, when  $(c_* \rightarrow 0, p_* \rightarrow \xi)$  we obtain,  $r_*^C \rightarrow r^C, r_*^P \rightarrow r^P$ , regardless of,  $\epsilon \rightarrow 0, 1$ . For high thresholds the radius of the MVR is small but increases with decreasing  $\epsilon$ . It can equal the entanglement or connection radius for high thresholds and vanishing  $\epsilon$  or when the thresholds are low for any value of  $\epsilon$ .

*Width of the maximal viable region:* The difference of the radii of the MVR and TVR,  $\Delta(r_*, \epsilon) := (\tilde{r}_* - r_*)$ , measures the width of the MVR. For any,  $D$ , in this annular region relative to the node,  $S$ , the QIP thresholds can be probabilistically met with an upper bound on this probability of at least  $\epsilon$ . Assuming,  $\tilde{r}_* = \tilde{r}_*^C$  and  $r_* = r_*^C$ , the width scales as,  $\Delta(r_*, \epsilon) \sim r^C c_*(1 - \epsilon)$ . The width is proportional to the entanglement radius,  $r^C$ , for large thresholds,  $c_* \rightarrow 1$ , but suppressed for small thresholds by the factor,  $c_* \rightarrow 0$ .

For high thresholds, the radius of the TVR is small,  $r_* = r^C(1 - \ln(1 + 2c^*)/\ln 3) \ll r^C$ , and in this scenario the width  $\Delta(r_*, \epsilon)$  can be related to the width of the edge parameter

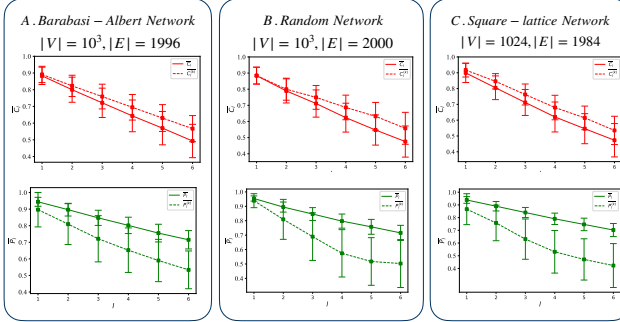


FIG. 2. Average path-parameters vs graph distance between  $S$ - $D$  nodes for various underlying graph topologies of a quantum network. The plots in solid and dotted Red (Green) are average path-concurrence (probability) for entanglement distribution using single paths and using multi-path purification respectively. The entanglement distributed along up to,  $k_{max} = 3$  distinct paths, subject to availability, were purified to obtain the path parameters in the multi-path scenario. All data points plotted (solid squares) are averages obtained by sampling 100- $D$  nodes relative to each of 100- $S$  nodes in networks with average edge-concurrence,  $\overline{\mu}_1 = 0.9$  and average edge-probability,  $\overline{\mu}_2 = 0.95$ .

distribution via,

$$\Delta(r_*, \epsilon) = \frac{r_*(1-\epsilon)(b_1 - a_1)}{1 - (1-\epsilon)b_1}, \quad (9)$$

which decreases with  $\epsilon$  but increases with  $r_*$  and the width,  $(b_1 - a_1)$ , of the edge concurrence distribution. This provides an interesting insight into the viability structure of a quantum network. For homogenous networks,  $(b_1 - a_1) \rightarrow 0$ , thus the TVR and MVR coincide,  $\tilde{V}_S \rightarrow V_S$  since  $\Delta(r_*, \epsilon) \rightarrow 0 \forall r_*, \epsilon$ . For heterogenous networks,  $(b_i - a_i) > 0$ , therefore, the TVR and MVR are distinct,  $V_S \subset \tilde{V}_S$ . Moreover, in this case viable regions have sharper boundaries for higher threshold tasks since  $\Delta(r_*, \epsilon) \propto r_*$ . Finally, notice that when,  $\epsilon \rightarrow 1$ , the MVR coincides with the TVR, that is,  $\tilde{V}_S \rightarrow V_S$  for any threshold,  $0 \leq c_* \leq 1$ . (See supp. mat.)

*Optimality of shortest graph paths for entanglement connections:* The axiomatic definition of the TVR, Eq. (5), based on entanglement connection along the SGP between any  $S$ - $D$  node pair can be justified by considering the probability that the SGP is optimal for entanglement distribution with respect to both path parameters,

$$\Pr(\text{SGP is optimal}) \geq \prod_{i=1}^2 \frac{1}{r_*(b_i - a_i) + b_i}, \quad (10)$$

where the RHS above is the product of the independent probabilities that the SGP maximizes the path concurrence and also that it maximizes the path probability for the entanglement distribution scheme described earlier. For homogenous networks,  $(b_i - a_i) \rightarrow 0, b_i \rightarrow 1$ , and,  $\Pr(\text{SGP is optimal}) \rightarrow 1 \forall r_*$ , which implies that the SGP maximizes both path parameters and is thus the unique element of the Pareto-optimal

set of paths between  $S$  and any  $D \in V_S$ . Whereas, in heterogeneous networks,  $(b_i - a_i) \neq 0, b_i > 1$ , thus the RHS in Ineq. (10) can be small implying that entanglement connections along paths other than the SGP between  $S$ - $D$  nodes may yield higher values of path parameters within the TVR,  $V_S$ . Therefore, for heterogenous QNs multi-objective shortest path algorithms for determining the full set of Pareto-optimal paths [26] and multi-path entanglement routing methods [16, 17] may be required to determine optimal entanglement connection paths.

*Purifying entanglement distributed along Pareto-optimal paths and Multi-path viable regions:* The TVR for a QIP task can be enlarged by purifying the entangled states obtained over distinct alternate paths,  $\mathcal{P}_{S-D}^k, k = 1, 2, \dots, k_{max}$ , between any given  $S$ - $D$ -node pair, see Fig. 1D. Each path provides, in general, a distinct isotropic state  $\rho^k$  between the end nodes of the form, Eq. (1). This set of  $k$  states can be sequentially pairwise-purified using Deutsch's protocol for entanglement pumping [27]. While the concurrence of the effective entanglement connection between  $S$ - $D$  can be increased in this manner, the effective probability actually decreases since we need entanglement connections along multiple distinct paths as well as the multiple purification steps to succeed, see Fig. 2 (and supp. mat.).

The multi-path TVR,  $V_S^{(k)}$  with radius  $r_*^{(k)}$ , for a QIP task about a random  $S$ -node can be defined as a generalization of Eq. (5) where we now require,  $(\overline{C}_l^{(k)}, \overline{P}_l^{(k)}) \geq (c_*, p_*)$ , with  $\overline{X}_l^{(k)}$ , ( $X = C, P$ ), the average effective parameter (over pairs of  $S$ - $D$  nodes) of the entanglement connection upon purifying the states obtained over  $k$ -distinct entanglement distribution paths between a  $S$ - $D$  pair at a graph distance of,  $l$ . Our analysis shows (see supp. mat.) that purification is useful to enlarge the TVR radius for high threshold tasks,  $(c_* \rightarrow 1, p_* \rightarrow 1)$ ,  $r_* \ll r^C, r^P$  and for a small number of paths,  $k \gtrsim 3$ , independent of the size of the network, because the effective concurrence,  $\overline{C}_l^{(k)}$ , saturates quickly with,  $k$ , while the effective probability,  $\overline{P}_l^{(k)}$ , decreases as  $\sim 1/k$ . In this case  $r_*^{(k)} = 3r_*$  for the parameter range,  $\overline{\mu}_1 < \overline{\mu}_2$ . For small threshold tasks,  $(c_* \rightarrow 0, p_* \rightarrow \xi)$ ,  $r_* \sim r^C, r^P$ , purification is not effective in boosting the concurrence of the entanglement connection since the average path concurrence at such graph distances relative to,  $S$ , is small,  $\overline{C}_l \approx 0$ , implying that,  $\overline{C}_l^{(k)} \approx 0$ ; moreover, the effective path probability degrades rapidly as  $\sim 1/k$  also in this region, so that  $r_*^{(k)} \leq r_*$ .

Multi-path entanglement purification is therefore effective for high-threshold QIP tasks that are viable in the vicinity of a random source node,  $S$ . In this region, although the viability radius can be increased only by a small factor independent of graph size or mildly-dependent on the number of paths purified - it can still bring a large number of destination nodes within the effective TVR,  $V_S^{(k)}$ , if implemented around the hubs of a QN with scale-free topology [25].

*Topography of the quantum internet:* We now apply our

results to a photonic QN based on an underlying soft random geometric graph recently considered in [6]. Here, the probability for two nodes at Euclidean-distance  $z$  to share an edge and have a photonic connection,  $P(z) = e^{-z/2\alpha R}[1 - (1 - 10^{-\gamma z/10})^{n_p}]$ , depends on the model parameters,  $\alpha = 226/2R$ ,  $\gamma = 0.2$  dB/km - that control the typical edge-length and fiber-loss, respectively and  $n_p$  the number of photons used per entanglement generation attempt. For such a network with  $N = 1500$  nodes distributed uniformly randomly over an area of radius  $R = 10^3$  kms, the node density,  $\rho = 3.18 \times 10^{-4}$  per sq. km, is above the critical density,  $\rho_c = 6.82 \times 10^{-5}$  per sq. km, implying that the network is connected satisfying the requirements for our topographical analysis. Further, the average graph-distance between any two nodes is,  $\langle l \rangle_{QN} \approx b\sqrt{N}/\rho = 4$ , where  $b = 5 \times 10^{-5}$  is a numerically estimated parameter.

We ask whether it is viable to perform point-to-point QKD in this photonic QN for arbitrary  $S$ - $D$  node pairs? That is, for what target edge-parameter distributions,

$$r_* \geq \langle l \rangle_{QN}. \quad (11)$$

Solving this inequality gives us,  $\overline{\mu_1} \approx 0.95$  and  $\overline{\mu_2} \approx 0.405$ , for  $n_p = 10^6$  (see supp. mat.) implying that QKD at secure-key generation rate of  $R_{sec} = 1$  kHz is viable between arbitrary  $S$ - $D$  nodes in this QN on-average, with 1 MHz entanglement generation sources and channels that produce states with an average concurrence of 0.95. A simple calculation of the typical viability radius can therefore estimate the functionality of the quantum network and identify target experimental parameters. (See supp. mat. for details)

*Discussion and conclusions:* We showed that entanglement topography reveals important functional information and provides experimental targets for the edge parameters to obtain large-scale quantum networks of arbitrary topologies. Relevant for applications, the typical and maximal regions indicate the viability of QIP tasks, guide the choice of optimal entanglement distribution paths and the utility of complex network operations and protocols such as entanglement purification and multi-path entanglement routing.

The topography uncovered here was relative to a plausible, but specific, entanglement distribution scheme which can be generalised to other scenarios, for example, when the network comprises of quantum repeater type links [11],[28]. Further, the effect of multi-path [16, 17] and multi-commodity flow [29] strategies in enhancing the viability region for different graph topologies needs to be analysed. Finally, the robustness of these viable regions to node and link failures of the quantum network needs to be understood since the network connectivity seems to be prone to discontinuous phase transitions under such events [8, 30]. In the future, we hope to explore the distinct topography for different quantum network topologies which can help in efficient quantum network design.

*Acknowledgements:* SS would like to acknowledge useful conversations with David Elkouss at OIST and funding from DST, Govt. of India through the SERB grant

MTR/2022/000389, IITB TRUST Labs grant DO/2023-SBST002-007 and the IITB seed funding.

\* Corresponding author: [santra@iitb.ac.in](mailto:santra@iitb.ac.in)

- [1] S. Pirandola and S. L. Braunstein, *Nature* **532**, 169 (2016).
- [2] S. Wehner, D. Elkouss, and R. Hanson, *Science* **362** (2018).
- [3] C. Simon, *Nature Photonics* **11**, 678 (2017).
- [4] P. Kómár, E. M. Kessler, M. Bishof, L. Jiang, A. S. Sørensen, J. Ye, and M. D. Lukin, *Nature Physics* **10**, 582 (2014).
- [5] J. Yin, Y.-H. Li, S.-K. Liao, M. Yang, Y. Cao, L. Zhang, J.-G. Ren, W.-Q. Cai, W.-Y. Liu, S.-L. Li, R. Shu, Y.-M. Huang, L. Deng, L. Li, Q. Zhang, N.-L. Liu, Y.-A. Chen, C.-Y. Lu, X.-B. Wang, F. Xu, J.-Y. Wang, C.-Z. Peng, A. K. Ekert, and J.-W. Pan, *Nature* **582**, 501 (2020).
- [6] S. Brito, A. Canabarro, R. Chaves, and D. Cavalcanti, *Phys. Rev. Lett.* **124**, 210501 (2020).
- [7] Q. Zhuang and B. Zhang, *Phys. Rev. A* **104**, 022608 (2021).
- [8] B. C. Coutinho, W. J. Munro, K. Nemoto, and Y. Omar, *Communications Physics* **5**, 105 (2022).
- [9] X. Meng, J. Gao, and S. Havlin, *Phys. Rev. Lett.* **126**, 170501 (2021).
- [10] K. Azuma, S. Bäuml, T. Coopmans, D. Elkouss, and B. Li, *AVS Quantum Science* **3** (2021), 10.1116/5.0024062.
- [11] K. Azuma, S. E. Economou, D. Elkouss, P. Hilaire, L. Jiang, H.-K. Lo, and I. Tzitrin, “Quantum repeaters: From quantum networks to the quantum internet,” (2023), [arXiv:2212.10820 \[quant-ph\]](https://arxiv.org/abs/2212.10820).
- [12] R. V. Meter, R. Satoh, N. Benchasattabuse, K. Teramoto, T. Matsuo, M. Hajdusek, T. Satoh, S. Nagayama, and S. Suzuki, in *IEEE International Conference on Quantum Computing and Engineering, QCE 2022, Broomfield, CO, USA, September 18-23, 2022* (IEEE, 2022) pp. 341–352.
- [13] M. Brekenfeld, D. Niemietz, J. D. Christensen, and G. Rempe, *Nature Physics* **16**, 647 (2020).
- [14] P. Hansen, in *Multiple Criteria Decision Making Theory and Application*, edited by G. Fandel and T. Gal (Springer Berlin Heidelberg, Berlin, Heidelberg, 1980) pp. 109–127.
- [15] E. Q. V. Martins, *European Journal of Operational Research* **16**, 236 (1984).
- [16] M. Pant, H. Krovi, D. Towsley, L. Tassiulas, L. Jiang, P. Basu, D. Englund, and S. Guha, *npj Quantum Information* **5**, 25 (2019).
- [17] H. Leone, N. R. Miller, D. Singh, N. K. Langford, and P. P. Rohde, “Qunet: Cost vector analysis & multi-path entanglement routing in quantum networks,” (2021), [arXiv:2105.00418 \[quant-ph\]](https://arxiv.org/abs/2105.00418).
- [18] P. Contreras-Tejada, C. Palazuelos, and J. I. de Vicente, *Phys. Rev. Lett.* **128**, 220501 (2022).
- [19] S. Santra, S. Muralidharan, M. Lichtman, L. Jiang, C. Monroe, and V. S. Malinovsky, *New Journal of Physics* **21**, 073002 (2019).
- [20] M. Caleffi, *IEEE Access* **5**, 22299 (2017).
- [21] Y. Ismail, S. Joshi, and F. Petruccione, *Scientific Reports* **7**, 12091 (2017).
- [22] J. A. Bergou, D. Fields, M. Hillery, S. Santra, and V. S. Malinovsky, *Phys. Rev. A* **104**, 022425 (2021).
- [23] C. H. Bennett, G. Brassard, S. Popescu, B. Schumacher, J. A. Smolin, and W. K. Wootters, *Phys. Rev. Lett.* **76**, 722 (1996).
- [24] J.-W. Pan, S. Gasparoni, R. Ursin, G. Weihs, and A. Zeilinger, *Nature* **423**, 417 (2003).

- [25] R. Cohen and S. Havlin, *Phys. Rev. Lett.* **90**, 058701 (2003).
- [26] D. fields, S. Santra, *In preparation*.
- [27] D. Deutsch, A. Ekert, R. Jozsa, C. Macchiavello, S. Popescu, and A. Sanpera, *Phys. Rev. Lett.* **77**, 2818 (1996).
- [28] S. Santra, L. Jiang, and V. S. Malinovsky, *Quantum Science and Technology* **4**, 025010 (2019).
- [29] K. Azuma, “Networking quantum networks with minimum cost aggregation,” (2023), [arXiv:2304.08921 \[quant-ph\]](https://arxiv.org/abs/2304.08921).
- [30] B. Zhang and Q. Zhuang, *Quantum Science and Technology* **6**, 045007 (2021).
- [31] L. de Mesnard, *SSRN* (2020), <http://dx.doi.org/10.2139/ssrn.3523802>.

## SUPPLEMENTARY MATERIAL

### PATH PARAMETERS OF AN ENTANGLEMENT CONNECTION

The entanglement connection along any network path is realized via entanglement swapping at all intermediate stations. In our case two path parameters are of interest: the path concurrence and the path probability, both of which we derive in the following.

*Path concurrence:* At a particular node swapping can be performed on states,  $\rho_{e_1}, \rho_{e_2}$ , both of the form,

$$\rho_{e_{1,2}} = (1 - q_{e_{1,2}}) |\phi^+\rangle \langle \phi^+| + q_{e_{1,2}} \frac{\mathbf{1}_4}{4}, \quad (12)$$

by projectively measuring the two qubits at the common node between the edges, one from each entangled pair, in a complete basis of the Bell states  $|\beta\rangle = |\phi_{\pm}\rangle, |\psi_{\pm}\rangle$  where  $|\phi_{\pm}\rangle = (|00\rangle \pm |11\rangle)/\sqrt{2}$  and  $|\psi_{\pm}\rangle = (|01\rangle \pm |10\rangle)/\sqrt{2}$ . This results in the post swapped state  $\rho(\tilde{q})$  of the same form (up to local unitaries) as Eq. (12) but with the effective state parameter,

$$\tilde{q} = (q_{e_1} + q_{e_2} - q_{e_1} q_{e_2}) = 1 - (1 - q_{e_1})(1 - q_{e_2}), \quad (13)$$

All four outcomes corresponding to the different  $|\beta\rangle$  are equiprobable and all four outcomes have the same concurrence of the post-swap state given by  $C(\rho_{swapped}) = (1 - \frac{3}{2}\tilde{q})$ . This calculation is done explicitly in reference [22].

For evaluating the end-to-end concurrence of a path,  $\mathcal{P}$ , comprised of  $l$ -edges obtained by entanglement-swapping at all intermediate stations, we iterate Eq. (13) to obtain the effective state parameter for path of length  $l$  with states  $\rho_{e_i}, i = 1, \dots, l$  along the edges as,

$$q_{\mathcal{P}} = 1 - \prod_{i=1}^l (1 - q_{e_i}). \quad (14)$$

Since the edge parameters are assumed to be i.i.d. over the  $l$ -edges in the path, the average path parameter,  $\bar{q}_{\mathcal{P}} = 1 - (1 - \bar{q})^l$ . Therefore, we can evaluate the exact path-concurrence in terms of the average edge-concurrence as,

$$\bar{C}_l = \text{Max}[0, \frac{3}{2} \frac{(1 + 2\bar{\mu}_1)^l}{3^l} - \frac{1}{2}], \quad (15)$$

by noticing that the average concurrence over any edge,  $\bar{\mu}_1 = \text{Max}[0, 1 - 3/2\bar{q}] = (1 - 3/2\bar{q})$  for  $0 \leq \bar{q} \leq 2/3$ , that is, in this range the edge-concurrence and state parameter are linearly related. Since, in our parametrisation,  $\bar{\mu}_1 = (1 - \delta_1)$ , we can also write,

$$\bar{C}_l = \text{Max}[0, \frac{3}{2} (1 - (2/3)\delta_1)^l - \frac{1}{2}]. \quad (16)$$

For large-scale networks of size  $N \rightarrow \infty$ , we need  $\delta_1 \sim 1/\text{Poly}(N) \rightarrow 0$ . Therefore, we get the behavior of  $\bar{C}_l$  for short- and long- path lengths,  $l$  as,

$$\begin{aligned} \bar{C}_l &\simeq (1 - l\delta_1), \quad l \ll (1/\delta_1) = \text{Poly}(N) \\ \bar{C}_l &= \frac{3}{2} e^{-(2/3)\delta_1 l} - \frac{1}{2}, \quad l \gtrsim \frac{3 \ln 3}{2 \delta_1} := r^C \sim \text{Poly}(N) \end{aligned} \quad (17)$$

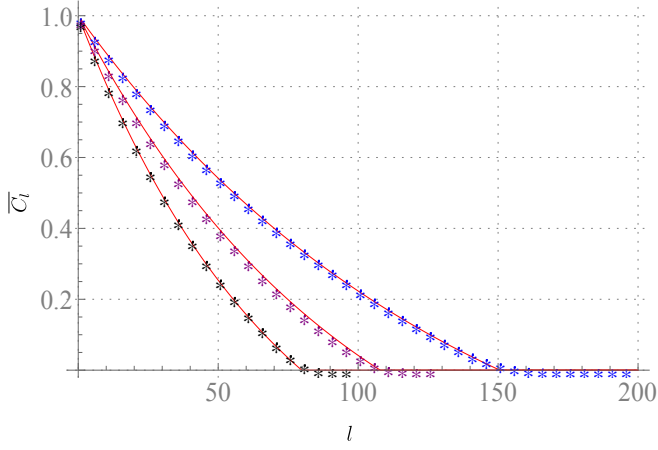


FIG. 3. (left) Simulated average concurrence (stars) vs path length in networks with different entanglement radii:  $r^C = 164$ ,  $\bar{r}_1 = 0.99$  (Blue),  $r^C = 109$ ,  $\bar{r}_1 = 0.985$  (Purple),  $r^C = 82$ ,  $\bar{r}_1 = 0.98$  (Black). Smooth red line shows the analytical result. In all cases  $10^4$  random paths were sampled.

Notice that the average concurrence for a path decreases monotonically with its length. The decrease is linear for short graph distances but exponentially suppressed at path lengths that are comparable to the entanglement radius of the network. This is shown in Fig. 3.

*Path concurrence:* The path probability in the entanglement distribution scheme is simply a product of the edge probabilities  $P_{\mathcal{P}} = \prod_e p_e$ , therefore the average path probability for a path of length  $l$  where the edge probabilities are i.i.d. is,

$$\bar{P}_l = \prod_{e \in \mathcal{P}} \bar{p}_e = (\bar{p}_2)^l = (1 - \delta_2)^l. \quad (18)$$

The behavior of  $\bar{P}_l$  for short- and long- path lengths,  $l$ , is thus,

$$\begin{aligned} \bar{P}_l &\simeq (1 - l\delta_2), \quad l \ll (1/\delta_2) = \text{Poly}(N) \\ \bar{P}_l &\simeq e^{-\delta_2 l}, \quad l \simeq (1/\delta_2) = \text{Poly}(N) \end{aligned} \quad (19)$$

Again, notice that the average probability for a path decreases monotonically with its length. The decrease is linear for short graph distances but exponentially suppressed at path lengths that are comparable to the connection radius,  $r^P = \ln(1/\xi)/\delta_2$ , of the network, where  $1 \geq \xi > 0$  is some cutoff probability.

#### TYPICAL AND MAXIMAL VIABLE REGIONS - RADIUS AND WIDTH

##### Radius of the Typical Viable Region

To estimate the radius of the typical viable region,  $V_S$ , about a random node,  $S$ , in the graph let us recall the definition of

the TVR,

$$\begin{aligned} V_S &:= \{G_S \subseteq G \mid \mathcal{D}(S, D) \leq r_* \forall D \in G_S\}, \\ r_* &:= \text{largest } l \text{ s.t. } (\bar{C}_l, \bar{P}_l) \geq (c_*, p_*), \end{aligned} \quad (20)$$

where, the second line implies that the averages of the random-valued path parameters,  $X_l$ , with  $X = C, P$ , needs to be above the thresholds  $(c_*, p_*)$  within the entire TVR. Now, the average of  $X_l$  depends on the path length  $l$  and the mean values of the edge parameters  $\mu_1$  or  $\mu_2$ . Writing the path concurrence from the second line of Eq. (17) as  $\bar{C}_l = \frac{3}{2}e^{-(l/r^C) \ln 3} - \frac{1}{2}$ , where as previously defined  $r^C = (3/2) \ln 3/\delta_1$ , requiring  $\bar{C}_l \geq c_*$  gives us the maximum graph distance,  $l$ ,

$$l \leq r_*^C := r^C (1 - \ln(1 + 2c_*)/\ln 3). \quad (21)$$

Similarly, requiring  $\bar{P}_l = e^{-\delta_2 l} \geq p_*$  implies a maximum graph distance,

$$l \leq r_*^P := \ln(1/p_*)/\delta_2 = r^P \ln p_*/\ln \xi, \quad (22)$$

where,  $r^P = \ln(1/\xi)/\delta_2$ . Here,  $0 \leq \xi \leq 1$ , is some cutoff path probability above which the end nodes of the path may be considered to be connected.

The radius of the typical viable region is therefore,

$$r_* = \text{Min}(r_*^C, r_*^P) \quad (23)$$

##### Radius of the Maximal Viable Region

To estimate the radius of the maximal viable region,  $\tilde{V}_S$ , around a random graph node  $S$  let us recall its definition,

$$\begin{aligned} \tilde{V}_S &:= \{\tilde{G}_S \subseteq G \mid \mathcal{D}(S, D) \leq \tilde{r}_* \forall D \in \tilde{G}_S\} \\ \tilde{r}_* &:= \text{largest } l \text{ s.t. } \text{Max}(\Pr(C_l \geq c_*)) \geq \epsilon^C \\ &\quad \& \text{Max}(\Pr(P_l \geq p_*)) \geq \epsilon^P. \end{aligned} \quad (24)$$

The region,  $\tilde{V}_S$  is clearly obtained as the intersection of the regions  $\tilde{V}_S^C$  and  $\tilde{V}_S^P$  where the upper bound on the relevant path parameter satisfying the respective thresholds are independently satisfied. That is, the maximal viable region  $\tilde{V}_S^C$  for the path concurrence may be defined as,

$$\begin{aligned} \tilde{V}_S^C &:= \{\tilde{G}_S^C \subseteq G \mid \mathcal{D}(S, D) \leq \tilde{r}_*^C \forall D \in \tilde{G}_S^C\} \\ \tilde{r}_*^C &:= \text{largest } l \text{ s.t. } \text{Max}(\Pr(C_l \geq c_*)) \geq \epsilon^C, \end{aligned} \quad (25)$$

and similarly, the maximal viable region  $\tilde{V}_S^P$  for the path probability may be defined as,

$$\begin{aligned} \tilde{V}_S^P &:= \{\tilde{G}_S^P \subseteq G \mid \mathcal{D}(S, D) \leq \tilde{r}_*^P \forall D \in \tilde{G}_S^P\} \\ \tilde{r}_*^P &:= \text{largest } l \text{ s.t. } \text{Max}(\Pr(P_l \geq p_*)) \geq \epsilon^P. \end{aligned} \quad (26)$$

The radius,  $\tilde{r}_*$ , of  $\tilde{V}_S$  is therefore,

$$\tilde{r}_* = \text{Min}(\tilde{r}_*^C, \tilde{r}_*^P). \quad (27)$$

To obtain the radii of the maximal viable regions for the respective path parameters, we use the upper bound on the probability given by the Markov's inequality applied to the random-valued path parameter  $X_{\tilde{l}}$  and find the largest  $\tilde{l}$  for which the Inequality is saturated. The probability of  $X_{\tilde{l}}$  to be greater than its threshold value,  $x_*$ , is lower bounded by  $\epsilon^X$  by definition of the maximal viable regions in Eqs. (25) and (26). Thus we seek the largest  $\tilde{l}$  for which,

$$\epsilon^X \leq \Pr(X_{\tilde{l}} \geq x_*) \leq \overline{X_{\tilde{l}}}/x_*. \quad (28)$$

Using Eqs. (17) and (19) we get the maximum  $\tilde{l}$  for which the above condition holds for the two different path parameters, the path concurrence and the path probability, giving us the corresponding radii of the two regions  $\tilde{V}_S^C, \tilde{V}_S^P$ ,

$$\begin{aligned} \tilde{l} \leq \tilde{r}_*^C &:= \leq r^C (1 - \ln(2c_* \epsilon^C + 1) / \ln 3), \\ \tilde{l} \leq \tilde{r}_*^P &:= \leq r^P \ln(p_* \epsilon^P) / \ln(\xi). \end{aligned} \quad (29)$$

Note that using this method the radii depend on the edge parameter distributions only via their averages,  $\overline{\mu_1}$  and  $\overline{\mu_2}$ .

### Width of the maximal viable region - I

The width,  $\Delta(r_*, \epsilon)$ , of the typical viable region is the magnitude of the difference between the radii of the maximal viable region,  $\tilde{V}_S$ , and that of the typical viable region  $V_S$ . Thus,

$$\begin{aligned} \Delta(r_*, \epsilon) &:= \tilde{r}_* - r_* \\ &= \text{Min}(\tilde{r}_*^C, \tilde{r}_*^P) - \text{Min}(r_*^C, r_*^P), \\ &= \text{Min}(\tilde{r}_*^C - r_*^C, \tilde{r}_*^C - r_*^P, \tilde{r}_*^P - r_*^C, \tilde{r}_*^P - r_*^P), \end{aligned} \quad (30)$$

where,  $\epsilon = \text{Min}(\epsilon^C, \epsilon^P)$ . The minimum in the second line above depends on the means  $\overline{\mu}_{1,2}$  and the values of  $\epsilon^C, \epsilon^P$  as can be seen from Eqs. (21), (22) and (29).

Assuming  $\Delta(r_*, \epsilon) = (\tilde{r}_*^C - r_*^C)$  and  $\epsilon = \epsilon^C$  is the minimum among the four values the width can be estimated to be,

$$\begin{aligned} \Delta(r_*, \epsilon) &= r^C \left(1 - \frac{\ln(1 + 2c_* \epsilon)}{\ln 3}\right) - r^C \left(1 - \frac{\ln(1 + 2c_*)}{\ln 3}\right) \\ &= r^C \ln \left[ \frac{(1 + 2c_*)}{(1 + 2c_* \epsilon)} \right]. \end{aligned} \quad (31)$$

In the various regimes of  $c_*$  and  $\epsilon$ , we see that,

$$\begin{aligned} \Delta(r_*, \epsilon) &\simeq 2r^C c_*(1 - \epsilon), \quad c_* \rightarrow 0 \text{ \& } 0 \leq \epsilon \leq 1 \\ &\simeq r^C (\ln 3 - 2\epsilon), \quad c_* \rightarrow 1 \text{ \& } \epsilon \rightarrow 0 \\ &\simeq (2/3)r^C (1 - \epsilon), \quad c_* \rightarrow 1 \text{ \& } \epsilon \rightarrow 1 \end{aligned} \quad (32)$$

The width is therefore proportional to the radius of the typical viable region and linearly decreases with increasing values of  $\epsilon$ .

### Width of the maximal viable region - II

The width of the TVR in Eq. (30) is obtained in terms of the means of the edge parameter distributions. However, use of another technique connects the width to additional statistical descriptors of the latter. Namely, it shows the direct proportionality of the width of the TVR to the width of the edge parameter distributions themselves.

This other way of estimating,  $\Delta^X(r_*^X, \epsilon^X)$ , is by considering the (positive indefinite) random variable,

$$Y_{l,d} := (X_{l,d} - X_l), \quad (33)$$

which is the difference of path parameters along two network paths of length  $(l + d)$  and  $l$ . Then,  $\Pr(Y_{l,d} \geq 0) = \Pr(X_{l,d} \geq X_l)$  for  $l = r_*^X$ , is an overestimate of  $\Pr(X_{r_*^X + d} \geq x_*)$  since,

$$\begin{aligned} \Pr(X_{l,d} \geq X_l)|_{l=r_*^X} &= \Pr(X_{r_*^X + d} \geq X_{r_*^X})|_{X_{r_*^X} \geq x_*} \\ &\quad + \Pr(X_{r_*^X + d} \geq X_{r_*^X})|_{X_{r_*^X} < x_*}, \end{aligned} \quad (34)$$

where, the first term on the right hand side of the equation is the probability that the path of length  $(r_*^X + d)$  satisfies the threshold for the parameter  $X$ . The maximum,  $d$ , for which the upper bound on the probability,  $\Pr(X_{r_*^X + d} \geq x_*)$ , is greater than  $\epsilon^X$  gives the width of the maximal viable region.

A generalization of Markov's inequality [31] to positive indefinite random variables yields,

$$\Pr(Y_{l,d} \geq 0) \leq 1 - \overline{Y_{l,d}}/(y_{l,d})_m, \quad (35)$$

with,  $(y_{l,d})_m$  the minimum value of  $Y_{l,d}$ , where the R.H.S. of the inequality above upper bounds the probability expressed in Eq. (34).

Note that the minimum,  $(y_{l,d})_m$ , and maximum,  $(y_{l,d})_M$ , and mean value  $\overline{Y_{l,d}}$  of  $Y_{l,d}$  for  $X = C$  is given by,

$$\begin{aligned} (y_{l,d})_m &= \frac{3}{2} \left[ \left(1 - \frac{2}{3}a_1\delta_1\right)^{l+d} - \left(1 - \frac{2}{3}b_1\delta_1\right)^l \right], \\ (y_{l,d})_M &= \frac{3}{2} \left[ \left(1 - \frac{2}{3}b_1\delta_1\right)^{l+d} - \left(1 - \frac{2}{3}a_1\delta_1\right)^l \right], \\ \overline{Y_{l,d}} &= \frac{3}{2} \left[ \left(1 - \frac{2}{3}\delta_1\right)^l \left\{ \left(1 - \frac{2}{3}\delta_1\right)^d - 1 \right\} \right], \end{aligned} \quad (36)$$

and it turns out that  $(y_{l,d})_m \leq 0$  and  $(y_{l,d})_M \geq 0$  and  $\overline{Y_{l,d}} \leq 0$  for all  $d \geq 1$  and  $l \geq 1$  when  $\delta_1 \sim 1/\text{Poly}(N) \rightarrow 0$ . Thus, the ratio,  $\overline{Y_{l,d}}/(y_{l,d})_m$ , is positive and the upper bound in the RHS of Ineq. (35) is non-trivial for,  $\overline{Y_{l,d}} < 0$ . Moreover, for small  $\delta_1$ ,

$$\begin{aligned} \overline{Y_{l,d}} &\simeq -d\delta_1 + O(\delta_1^2), \\ (y_{l,d})_m &= -\delta_1 \{l(b_1 - a_1) + db_1\} + O(\delta_1^2) \end{aligned} \quad (37)$$

The Ineq. (35) therefore implies that,

$$\Pr(C_{l,d} \geq C_l) \leq 1 - \frac{d}{l(b_1 - a_1) + db_1}, \quad (l + d) \ll r^C, \quad (38)$$

the R.H.S. of which is a monotonically decreasing function of  $d$  for a fixed  $l, a_1, b_1$ . Requiring  $\Pr(C_{l,d} \geq C_l) \geq \epsilon$  for  $l = r_*^C$  and solving for  $d$  using the RHS of the equation above we get,

$$\Delta(r_*^C, \epsilon) = \frac{r_*^C(1-\epsilon)(b_1 - a_1)}{1 - (1-\epsilon)b_1}, \quad (39)$$

Since Eq. (??) is derived under the assumption,  $0 \leq \Delta(r_*, \epsilon) \ll r^C, r^P$ , the range of  $\epsilon$  is bounded,  $(1 - 1/b) \leq \epsilon \leq 1$ .

A similar analysis for path probabilities using the random variable  $Z_{l,d} := P_{l+d} - P_l$  where  $Z_{l,d} \in [(z_{l,d})_m, (z_{l,d})_M]$  implies that,

$$\begin{aligned} \Pr(P_{l,d} \geq P_l) &\leq 1 - \frac{\overline{Z_{l,d}}}{(z_{l,d})_m} \\ &= 1 - \frac{d}{l(b_2 - a_2) + db_2}, \quad (l + d) \ll r^P, \end{aligned} \quad (40)$$

and  $\overline{Z_{l,d}} = \bar{p}^{l+d} - \bar{p}^l$  whereas  $(z_{l,d})_m = p_m^{l+d} - p_M^l$ . Requiring that,  $\Pr(P_{l,d} \geq P_l) \leq \epsilon$ , for  $l = r_*^P$  leads to the equation,

$$\Delta(r_*^P, \epsilon) = \frac{r_*^P(1-\epsilon)(b_2 - a_2)}{1 - (1-\epsilon)b_2}. \quad (41)$$

The equations (39) and (41) imply that the width of the maximal viable regions for concurrence and probability depend on the widths of the respective distributions  $(b_i - a_i)$ ,  $i = 1, 2$ . Further, in agreement with Eq. (32), the widths are proportional to the radius of the typical viable regions via,  $r_*^C, r_*^P$ ; moreover, the width decreases for increasing values of  $\epsilon$  since  $\Delta(r_*, \epsilon) \sim (1-\epsilon)$ . For,  $\epsilon \rightarrow 1$  the width of the maximal viable region vanishes since the maximal and typical viable regions coincide.

#### TYPICAL AND MAXIMAL VIABLE REGIONS WITH MULTI-PATH ENTANGLEMENT PURIFICATION

In the main text we define the typical and maximal viable regions of the quantum network by studying the topography relative to a single path between  $S$ - $D$  for entanglement distribution as given by Eqs. (5) and (7). However, the network operation of entanglement purification can help purify the entanglement resources distributed via multiple distinct (no common edge) alternate paths,  $\mathcal{P}^k, k = 1, 2, \dots, k_{max}$ , between a given  $S$ - $D$  pair - potentially boosting their entanglement connection, see Fig. 4. The maximum number of such paths,  $k_{max}$ , that may be usefully purified is determined by the EP protocol or the topology of the network or both. For example, one choice for the number of distinct paths could be  $k_{max} = \text{Min}(\text{Deg}(S), \text{Deg}(D))$ , that is, the maximum number of distinct paths is only limited by the smaller among the degree of the  $S$  or  $D$  nodes.

The different distinct paths  $\mathcal{P}^k$  between nodes  $S, D$  distribute states  $\rho^k$ , all of which are isotropic states of the form

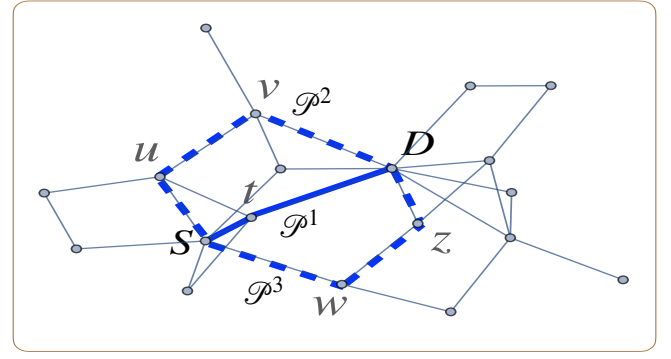


FIG. 4. Multiple distinct paths between a pair of end nodes  $S$ - $D$ . The path labeled  $\mathcal{P}^1(S \leftrightarrow t \leftrightarrow D)$  is the shortest graph path between the end-nodes and the state distributed over  $\mathcal{P}^1$  is always included in the purification protocols we consider. The paths  $\mathcal{P}^2(S \leftrightarrow u \leftrightarrow v \leftrightarrow D)$ ,  $\mathcal{P}^3(S \leftrightarrow w \leftrightarrow z \leftrightarrow D)$  are longer and may be included in the purification protocol if doing so improves the concurrence.

Eq. (1), with distinct concurrence value in general. Since isotropic states are diagonal in the Bell-basis they can be purified using Deutsch's protocol for entanglement purification [27]. In general, the output of this process yields a mixed state which is equivalent to an isotropic state up to local unitary transformations. While the concurrence of the entanglement connection between  $S, D$  can be increased in this manner, the probability of the entanglement connection actually decreases because we need entanglement connections along multiple distinct paths available as well as the multiple purification steps to succeed.

In quantum networks where multi-path entanglement purification over distinct alternate paths between a  $S, D$ -pair of nodes are allowed, we can define the multi-path typical viable region,  $V_S^{(k)}$ , for a quantum information processing task as the connected subgraph  $G_S^{(k)}$  centered at the node  $S$  such that,

$$\begin{aligned} V_S^{(k)} &:= \{G_S^{(k)} \subseteq G \mid \mathcal{D}(S, D) \leq r_*^{(k)} \forall D \in G_S^{(k)}\}, \\ r_*^{(k)} &:= \text{largest } l \text{ s.t. } (\overline{C_l^{(k)}}, \overline{P_l^{(k)}}) \geq (c_*, p_*), \end{aligned} \quad (42)$$

where,  $\overline{X_l^{(k)}}$ , is the average concurrence or probability obtained by purifying the  $\rho^k$  states obtained on up to  $k \geq 1$  distinct alternate paths, including the SGP, between a  $S$ - $D$  pair separated by a graph distance of  $l$ . The multi-path maximal viable regions under EP,  $\tilde{V}_S^{(k)}$ , can then be defined as,

$$\begin{aligned} \tilde{V}_S^{(k)} &:= \{\tilde{G}_S^{(k)} \subseteq G \mid \mathcal{D}(S, D) \leq \tilde{r}_*^k \forall D \in \tilde{G}_S^{(k)}\}, \\ \tilde{r}_*^k &:= \text{largest } l \text{ s.t. } \text{Max}(\Pr(C_l^{(k)} \geq c_*)) \leq \epsilon^C \\ &\quad \& \text{Max}(\Pr(P_l^{(k)} \geq p_*)) \leq \epsilon^P. \end{aligned} \quad (43)$$

Clearly,  $V_S^{(k)} = V_S$  and  $\tilde{V}_S^{(k)} = \tilde{V}_S$  for  $k = 1$ . However, for  $k \geq 2$  the regions  $V_S^{(k)}, \tilde{V}_S^{(k)}$  are not uniquely defined because

one can choose different sets of  $(k-1)$  alternate paths other than the SGP from among  $\binom{(k_{max}-1)}{(k-1)}$  Pareto-optimal possibilities with parameter sets,  $(C_{\mathcal{P}^i}, P_{\mathcal{P}^i}), 1 \leq i \leq (k-1)$  that generally lack total ordering. In practice, a criteria may be set for choosing the alternate paths whose entanglement resources are combined, based on path lengths for example, and then the multi-path typical and maximal viable regions can be identified numerically for a given graph.

Analytically, one estimate of the radii of the multi-path typical and maximal viable regions can be obtained assuming that all of the  $k$ -distinct paths between a given  $S, D$ -pair at a graph distance of  $l$  have the same concurrence and probability parameters - equal to the average connection parameters along the SGP given by Eq. (3). When,  $k$ , such identical isotropic states are used in an entanglement pumping type scheme for purification then at short graph distances,  $l \ll r_E, r_P$ , we find that,

$$\begin{aligned} \overline{C_l^{(k)}} &= (1 - z_1 l \delta_1), \\ \overline{P_l^{(k)}} &= 1 - lk(z_2 \delta_1 + \delta_2), \end{aligned} \quad (44)$$

where,  $0 \leq z_1, z_2 \leq 1$ , are positive fractions that are  $\mathcal{O}(1)$  with respect to  $l$  and with a very mild dependence on  $k$ . A little algebra shows that for  $k \geq 3$  the values of  $z_1 \approx 1/3$  whereas  $z_2 \approx 1/2$ . In fact for  $k \geq 3$  the average value of concurrence at a given  $l$  converges quickly to its asymptotic value which is shown in the first of the equations above. The entanglement connection probability given in the second line is obtained by considering the probability that  $k$ -isotropic states are available and  $(k-1)$  entanglement pumping steps are successful. For a given  $l$ , this probability is calculated as,  $(\overline{P}_l)^k N_1 N_2 \dots N_{k-1}$ , where  $N_i$  is the success probability of the  $i$ 'th pumping step. The entanglement connection probability therefore decreases linearly with  $k$  for a fixed  $l$ . Further, note that this probability now depends on parameters of both distributions, the edge concurrence distribution via  $\delta_1$  as well as the edge probability distribution via  $\delta_2$  because entanglement distribution protocols with purification make the path parameters  $C_l, P_l$  dependent on each other.

The radius of the multi-path typical viable region with regards to the concurrence,  $V_S^{(k),C}$ , is estimated to be,  $r_*^{(k),C} = (1 - c_*)/z_1 \delta_1$ ; whereas the typical viable region with regards to the probability,  $V_S^{(k),P}$ , has a radius,  $r_*^{(k),P} = (1 - p_*)/k(z_2 \delta_1 + \delta_2)$ . The multi-path typical viable region for the concurrence, therefore, has a radius that can be potentially 3-times as large as that of networks where no purification is used, that is,  $r_*^{(k),C} = 3r_*^C$  for  $k \geq 3$ . Whereas the multi-path typical region for the probability has a radius that is  $1/1.5k$  times the radius of the same region in networks that do not utilize purification, that is,  $r_*^{(k),P} = (1/1.5k)r_*^P$ .

It is possible to estimate the number of paths that need to be included in multi-path purification process under the assumptions we have made: paths have the same parameters as the average parameter along the shortest graph path between the same end-nodes. Note that the radius of the multi-path typical

viable region is given by the minimum of the two radii, that is,  $r_*^{(k)} = \min(r_*^{(k),P}, r_*^{(k),C})$ . We assume that  $c_* = p_* \rightarrow 1$ ,  $\delta_1 \geq \delta_2$ , and  $r_*^{(k)} = r_*^{(k),P}$ ,  $r_* = r_*^C$ , then comparing with Eq. (6) we find that  $r_*^{(k)} \geq r_*$  if  $k \leq r_*^P/r_*^C \approx \delta_1/\delta_2 = (1 - \mu_1)/(1 - \mu_2)$ . Therefore, a simple function of the means of the distributions gives the maximum number of paths  $k$  between a pair of nodes that can be beneficially combined using purification to obtain multi-path typical viable regions larger than the typical viable region with single path entanglement distribution.

For longer graph distances where,  $l \sim r_E, r_P$ , purification is not effective in boosting the concurrence of the entanglement connection because the values of the path concurrence parameter at such graph distances is small, that is,  $C_l \approx 0$ ; moreover, the probability of the entanglement connection degrades rapidly with  $k$  as shown in the second line of Eq. (44). In effect, for QNs entanglement purification operations are mostly useful for short graph distances,  $l \ll r_E, r_P$ , where they can potentially enlarge the typical viable region.

Finally, notice that since we assumed all paths between a pair of  $S, D$  nodes had identical values of the path parameters, we have estimated the radius of the typical viable regions of an effectively homogenous network. Therefore, the multi-path typical viable radius and maximal viable radius are the same,  $r_*^{(k)} = \tilde{r}_*^{(k)}$ . The widths of the multi-path typical regions, under this assumption is zero, that is  $\Delta^{(k),X}(r_*^{(k)}, \epsilon^X) \rightarrow 0$  for any  $\epsilon^X > 0$ . Numerically, this assumption is not necessary and we can obtain the radii of both, the multi-path typical and maximal viable regions by numerically sampling a sufficient number of  $S, D$  pairs, choosing alternate paths between each pair of  $S, D$  nodes using some criteria and numerically computing the effective concurrence and probability connection between the end nodes.

## TOPOGRAPHY OF THE QUANTUM INTERNET MODEL

Recently, the statistical properties of a model for the quantum internet have been explored in Ref. [6]. There, the quantum internet has been modeled as a photonic QN based on an underlying soft random geometric graph. Two important observations from this work relevant for our calculations here are the following:

1. There is a connectivity phase-transition above a critical density,  $\rho_c$ , of nodes per unit area such that most nodes of the network become a part of the giant component.
2. Quantum networks based on an underlying photonic network deviate from the small-world property, however, the average node-to-node distance is small.

Observation number 1 above implies that the network connectedness requirement for our topographical analysis can be satisfied above the critical node density. Here, we assume a network radius of  $R = 10^3$  kms with  $N = 1500$  uniformly randomly distributed nodes. Then, the node density,

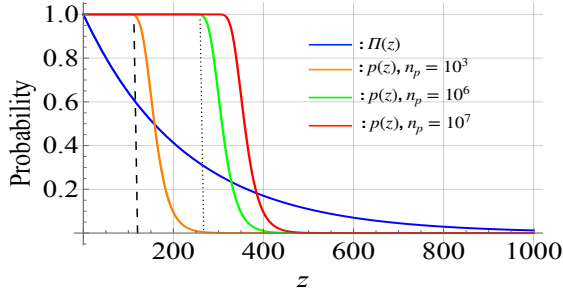


FIG. 5. (Color online) Probabilities vs. geographic distance in the photonic quantum network model. Shown in Blue is the probability,  $\Pi(z)$ , for any nodes to share an edge. Shown in Orange, Green and Red are the probabilities,  $p(z)$ , for a photonic connection to exist given that an edge exists between two nodes. In our calculations we use a step-function approximation for  $p(z)$  with  $p(z) = \Theta(L_{n_p} - z)$  with  $L_{n_p} = 250, 120$  (shown as vertical Brown dotted line, vertical Black dashed line) for  $n_p = 10^3, 10^6$  respectively.

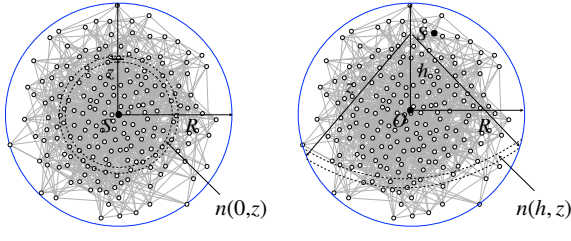


FIG. 6. (left) Simulated average concurrence (stars) vs path length in networks with different entanglement radii:  $r^C = 164, \bar{\mu}_1 = 0.99$  (Blue),  $r^C = 109, \bar{\mu}_1 = 0.985$  (Purple),  $r^C = 82, \bar{\mu}_1 = 0.98$  (Black). Smooth red line shows the analytical result. In all cases  $10^4$  random paths were sampled.

$\rho = N/\pi R^2 = 4.77 \times 10^{-4}$  nodes per sq. km, is above the critical density,  $\rho_c = 6.82 \times 10^{-5}$  nodes per sq. km, implying that the network is connected.

Observation number 2 is useful since numerical results obtained in Ref. [6] show that in the photonic QN, the average node-node separation in terms of graph distance scales as,

$$\langle l \rangle_{QN} = 5 \times 10^{-5} \sqrt{N}/\rho, \quad (45)$$

which for  $N = 1500$  and  $\rho = 4.77 \times 10^{-4}$  gives us  $\langle l \rangle_{QN} = 4$ . Therefore, if the typical viability radii is greater than this average node-node separation then an arbitrary pair of S-D nodes in the network will be able to perform the particular

task. That is, we want edge-parameter distributions such that,

$$r_* \geq \langle l \rangle_{QN}. \quad (46)$$

Recall now from Eq. (6) that,

$$r_* = \text{Min}\{r^C(1 - \frac{\ln(1+2c_*)}{\ln 3}), r^P \frac{\ln p_*}{\ln \xi}\}, \quad (47)$$

therefore, both  $r_*^C := r^C(1 - \frac{\ln(1+2c_*)}{\ln 3})$  and separately  $r_*^P := r^P \frac{\ln p_*}{\ln \xi}$  have to be greater than or equal to  $\langle l \rangle_{QN}$ . For the QIP task of QKD, we have  $(c_*, p_*) \geq (0.8, 1.6\%)$ . Thus, the edge-concurrence distribution in the photonic quantum network needs to have a mean,

$$\bar{\mu}_1 = 0.95 \implies r_*^C = 4. \quad (48)$$

To estimate,  $r_*^P$ , we need to estimate the mean edge-probability,  $\bar{\mu}_2$ , used in the description of the QN through, Eq. (2), in the main text. Unlike the mean edge-concurrence, the mean edge-probability is determined by the phenomenology of the photonic quantum network. We proceed as follows to calculate the mean edge-probability,

$$\bar{\mu}_2 = \mathcal{P}/\mathcal{N}, \quad (49)$$

where,  $\mathcal{P}$  is the sum of edge-probabilities over all edges of the network and  $\mathcal{N}$  is the total number of edges in the network. We can express the numerator and denominator above as,

$$\begin{aligned} \mathcal{P} &= \int_0^R P(h)n(0,h)dh \\ \mathcal{N} &= \int_0^R N(h)n(0,h)dh \end{aligned} \quad (50)$$

with,

$$\begin{aligned} P(h) &= \int_{z=0}^{R+h} n(h,z)\Pi(z)p(z)dz, \\ N(h) &= \int_{z=0}^{R+h} n(h,z)\Pi(z)dz, \end{aligned} \quad (51)$$

where, the expressions  $n(h,z)$ ,  $\Pi(z)$  and  $p(z)$  are explained sequentially below.

The term,  $n(h,z)$  is the number of points in an annular region between a radius of  $z$  and  $(z + dz)$  with the annulus centered at a point which is at a distance of  $h$  from the center of the network, see Fig. 6. We obtain,

$$n(h,z)dz = \begin{cases} 2\pi\rho z dz, & 0 \leq z \leq (R-h) \\ 2\rho \cos^{-1}(\frac{h^2+z^2-R^2}{2hz})dz, & (R-h) < z \leq (R+h) \end{cases} \quad (52)$$

There are two approximations we use in our calculation of Eq. (50). The first, is an approximation for the second line above where we use,  $\cos^{-1}(\frac{h^2+z^2-R^2}{2hz}) = \cos^{-1}(h/2R)$ . The second approximation is a step-function approximation for  $p(z)$  explained in the following paragraphs.

In our mathematical description of the QN in the main text, Eq. (2), the edge-probability is the product of the edge-connection probability,  $\Pi(z)$ , and the photonic-connection probability,  $p(z)$  used in the photonic QN model of Ref. [6]. The edge-connection probability,  $\Pi(z) = \beta e^{-z/2\alpha R}$ , is the probability that two nodes at a Euclidean-distance of  $z$ -kms are connected by an edge. Here, the value of  $2\alpha R$  km is the parameter value which determines the typical edge-length of the network and  $0 < \beta \leq 1$  determines the average node-degree. Following, Ref. [6] we use the estimates of  $\beta = 1$  and  $2\alpha R = 226$  for the U.S. fiber network.

The photonic-connection probability,  $p(z) = [1 - (1 - 10^{-\gamma z/10})^{n_p}]$ , is the probability that two nodes have a photonic connection given that an edge exists between. Here we take,  $\gamma = 0.2$  dB/km - which accounts for the fiber-loss with  $n_p$  the number of photons used per entanglement generation attempt. The behavior of  $p(z)$  is shown in Fig. 5 for different values of  $n_p$ . We notice that  $p(z)$  essentially stays constant for a maximum distance that depends on  $n_p$  after which it rapidly becomes zero. Therefore, we approximate  $p(z)$  as a

step function so that,

$$p(z) = \begin{cases} \Theta(250 - z), & n_p = 10^6 \\ \Theta(120 - z), & n_p = 10^3 \end{cases} \quad (53)$$

The above expressions yield the following values for  $\bar{\mu}_2$  and the corresponding value of  $r_*^P$  depending on the value of  $n_p$  when used in Eq. (51),

$$\bar{\mu}_2 = \begin{cases} 0.146, & r_*^P = 2, n_p = 10^3 \\ 0.404, & r_*^P = 4, n_p = 10^6 \end{cases} \quad (54)$$

From Eqs. (48) and (54) we get that, the *entire* photonic quantum network is a typical viable region for point-to-point QKD with a secure key generation rate of  $R_{sec} = 1$  kHz if 1 MHz entanglement photon pair sources are used in the network and it is assumed that the concurrence of the distributed states along the network edges has a mean of around 0.95.